

# Effect of differences in proton and neutron density distributions on fission barriers

J.F. Berger

Commissariat l'Energie Atomique, Service de Physique Nucléaire  
B.P. 12, 91680 Bruyres-le-Châtel, France

K. Pomorski

Theoretical Physics Department, University M.C.S., Lublin, Poland  
(November 18, 2018)

The neutron and proton density distributions obtained in constrained Hartree-Fock-Bogolyubov calculations with the Gogny force along the fission paths of  $^{232}\text{Th}$ ,  $^{236}\text{U}$ ,  $^{238}\text{U}$  and  $^{240}\text{Pu}$  are analyzed. Significant differences in the multipole deformations of neutron and proton densities are found. The effect on potential energy surfaces and on barrier heights of an additional constraint imposing similar spatial distributions to neutrons and protons, as assumed in macroscopic-microscopic models, is studied.

PACS numbers : 21.10.Dr, 21.10.Ft, 21.10.Gv, 24.75.+i, 25.85.Ca

Keywords: self-consistent theory, even-even nuclei, fission barriers

Experimental analyses of, e.g. electron and  $\alpha$ -particle scattering, pionic atoms, annihilation of antiprotons show that, in most nuclei, neutrons and protons have close but different r.m.s. radii [1]. The main reasons for this difference are unequal numbers of neutrons and protons, and the Coulomb interaction between protons.

In the last twenty-five years, fully microscopic approaches employing parameterized forms of the effective interaction between nucleons within a formalism of the Hartree-Fock type have been developed, which usually reproduce experimental proton and neutron r.m.s. radii and their difference in a satisfactory way [2–8]. Corrections coming from oscillations of the mean-field in principle have to be added, which slightly increase nucleon radii. However, they often may be neglected, except in a few closed shell nuclei and in nuclei exhibiting shape coexistence [9–11].

Experimental r.m.s. charge radii and isotopic shifts are also successfully reproduced by macroscopic-microscopic methods based on the liquid drop model and the Strutinsky shell correction technique [12–14]. Contrary to microscopic approaches, the proton and neutron mean-fields are not self-consistently determined, but taken as local potentials of prescribed forms – Nilsson or Saxon-Woods –, with identical spatial deformations.

In deformed nuclei, neutron and proton nuclear density distributions are expected to have not only different radii, but also different shapes, i.e. different quadrupole and higher multipole deformations. In Ref. [6], an analysis of theoretical densities based on a surface multipole moment expansion showed that significant differences between neutron and proton deformations often occur.

The aim of the present investigation is to check how large the differences between neutron and proton multipole deformations along paths to fission are, and to what extent fission barriers depend on such differences. This study is based on the constrained Hartree-Fock-Bogolyubov (HFB) approach with the Gogny effective interaction which has been extensively used several years ago to describe actinide fission [15]. Four well-known actinide nuclei,  $^{232}\text{Th}$ ,  $^{236}\text{U}$ ,  $^{238}\text{U}$  and  $^{240}\text{Pu}$  are considered.

Moments of the multipole components of the neutron and proton densities are first calculated as functions of quadrupole deformation using the method described in the next Section. In a second step, a constraint is introduced in the self-consistent calculation in order to impose identical spatial distributions to neutrons and protons. The resulting effect on the shape and height of fission barriers can be viewed as an estimate of the influence of the assumption usually made in macroscopic-microscopic Strutinsky type models (see e.g. [16–18]), that the neutron and proton potentials have the same multipole deformations.

The constrained HFB calculations have been performed following the method described in Ref. [15]. Axial symmetry of the nuclear shapes has been assumed. Nuclear deformation along fission paths has been generated by means of a linear constraint on the nuclear mass quadrupole moment  $\hat{Q}_{20} = \sum_{i=1}^A r_i^2 P_2(\cos \theta_i)$ . The two-body effective nucleon-nucleon interaction has been taken in the form proposed by Gogny [4], with the set of parameters D1S [19] adopted since 1983. Let us recall that this finite range effective force has been proved to give a very satisfactory *ab initio* description of the average field and pairing correlations in nuclei, and also of actinide fission barriers.

Generalized multipole moments  $Q_\lambda^k$  of the self-consistent density distributions  $\rho(\vec{r})$  are defined by the following integrals:

$$Q_\lambda^k = \int r^k P_\lambda(\cos \theta) \rho(\vec{r}) d^3 \vec{r} \quad (1)$$

where  $P_\lambda$  is a Legendre polynomial of order  $\lambda$ . The average  $\beta$ -deformation of multipole  $\lambda$  can be taken proportional to the ratio of the moment  $Q_\lambda^k$  to the monopole moment  $Q_0^k$ :

$$\beta_\lambda(k) = \frac{\sqrt{4\pi(2\lambda+1)}}{k+3} \frac{Q_\lambda^k}{Q_0^k}. \quad (2)$$

This definition yields deformation parameters close to the  $\beta_\lambda$  commonly used to define the shape of the nuclear surface in the liquid drop model :

$$R(\theta, \phi) = R_0(\{\beta_\lambda\}) \left( 1 + \sum_{\lambda=1}^m \beta_\lambda Y_{\lambda 0}(\theta, \phi) \right). \quad (3)$$

In particular, for small deviations from the sphere and for a uniform density distribution :

$$\beta_\lambda(k) = \beta_\lambda, \quad (4)$$

for any value of  $k$  in Eq. (1).

In Fig. 1, the fission barriers of  $^{232}\text{Th}$ ,  $^{236}\text{U}$ ,  $^{238}\text{U}$ , and  $^{240}\text{Pu}$  are plotted as functions of the mean value of the nucleus mass quadrupole moment  $\langle \hat{Q}_{20} \rangle$ . The solid line corresponds to left-right reflection symmetric nuclear shapes, while the dashed line represents the more general asymmetric case. As expected, fission barriers including asymmetric shapes are lower in these nuclei beyond the isomeric minimum. HFB energies along the fission paths have been corrected in the usual way [20] from the spurious zero-point energies associated with the fluctuations of the center of mass position, of the angular orientation and of the quadrupole deformation of the HFB states. Both one-body and two-body center of mass corrections have been computed. Let us mention that the lowering of the first hump of barriers due to triaxial instability is not included in the curves of Fig. 1.

The multipole deformation parameters: quadrupole  $\beta_2$ , octupole  $\beta_3$  and hexadecapole  $\beta_4$  defined by Eq. (2) have been evaluated along the different fission barriers of Fig. 1. As an example, the multipole deformations of the total nuclear density along the symmetric and asymmetric barriers of  $^{232}\text{Th}$  are plotted in the upper-left part of Fig. 2. In this analysis the surface multipole moment, i.e.  $k = 2$ , has been chosen. Deformations obtained with  $k = 4$  are not shown as they are close to those computed with  $k = 2$ .

Inserting neutron (resp. proton) density distributions into formula (1) allows one to get information about the neutron (resp. proton) multipole deformations. The other three diagrams in Fig. 2. display the differences  $\beta_\lambda^n - \beta_\lambda^p$  between neutron and proton deformations in  $^{232}\text{Th}$ . One observes that they strongly depend on deformation and are always negative for prolate deformations. Large values are obtained beyond the second minimum of the fission barrier, especially for octupole and hexadecapole deformations. There, the relative neutron-proton deformation difference  $|\beta_\lambda^n - \beta_\lambda^p|/\beta_\lambda$  reaches 4% in the quadrupole case, and exceeds 10% for  $\lambda = 3$  and 4.

The above neutron-proton differences exhibit a similar behavior in  $^{236}\text{U}$ ,  $^{238}\text{U}$  and  $^{240}\text{Pu}$ , although their magnitudes are not as large as in  $^{232}\text{Th}$ . As in the latter nucleus, the largest numbers are obtained for octupole and hexadecapole deformations. From these results one can conclude that the rearrangement of the nuclear structure along fission paths leads to an increase of the difference between neutron and proton deformations, the proton multipole deformations becoming significantly larger than neutron ones beyond the fission isomer potential minimum.

In order to estimate the influence on fission barriers of the differences found between the neutron and proton spatial distributions, the HFB calculations have been performed again, adding a new constraint ensuring that all multipole deformations  $\beta_\lambda(n)$  of protons and neutrons are equal. This has been done by imposing, at each iteration of the HFB procedure, that the neutron and proton density matrices are proportional to each other:

$$\rho_n = \frac{N}{Z} \rho_p \quad (5)$$

No such condition has been imposed on the neutron and proton pairing tensors.

As expected within a variational framework, the HFB energies computed with the additional constraint are found higher than those computed without this subsidiary condition. The differences  $\delta E_{\text{den}}$  between the HFB energies computed with and without the additional constraint along the fission paths of  $^{232}\text{Th}$ ,  $^{236-238}\text{U}$  and  $^{240}\text{Pu}$  are plotted in Fig. 3. As in Figs. 1 and 2, the solid lines represent the fission paths for reflection symmetric nuclear shapes, while the dashed lines correspond to reflection asymmetric ones. One can see that the  $\delta E_{\text{den}}$  differences are approximately 1.5 MeV on the average in  $^{240}\text{Pu}$  and  $^{236-238}\text{U}$ , with fluctuations having an amplitude of the order of 1 MeV. In  $^{232}\text{Th}$ , the average energy difference is slightly smaller, while stronger oscillations can be observed.

As a consequence, imposing condition (5) leads, in some cases, to an increase of fission barrier heights of  $\sim 1$  MeV. This can be seen in Fig. 4, where the fission barriers computed with (dashed line) and without (solid line) constraint (5) are plotted. Here, only the barriers corresponding to reflection asymmetric shapes are displayed. In order to better compare the two calculations, the dashed curves are shifted downward in order that the ground state minima in the dashed and solid curves coincide. One observes that, in spite of this shift, constraint (5) almost always leads to an increase of the heights of the barrier maxima and of the isomeric secondary minima. The biggest change occurs in  $^{238}\text{U}$ , where the height of the first barrier increases by 1 MeV. A smaller but sizable ( $\simeq .4 - .7$  MeV) increase of first barrier heights of the other three nuclei can be seen. In all nuclei except  $^{240}\text{Pu}$ , similar increases are obtained for second barriers and isomer well energies. In addition, the shape of the second barrier is slightly altered in  $^{232}\text{Th}$  and, to a lesser extent, in the other three nuclei.

In order to better illustrate the consequences of these barrier increases, their influence on spontaneous fission lifetimes has been estimated. Barrier penetration factors have been calculated using the WKB approximation, with collective inertia parameters computed from the method given in Ref. [21]. As a result, constraint (5) leads to spontaneous fission lifetimes increased by factors 9.8, 6.6, 22.4 and 2 in  $^{232}\text{Th}$ ,  $^{236}\text{U}$ ,  $^{238}\text{U}$  and  $^{240}\text{Pu}$ , respectively.

This work shows that the multipole deformations of the proton and neutron density distributions of fissioning nuclei are far from being equal. The relative difference between them often exceeds 10% and undergoes large variations. This means that the thickness of the neutron skin does not remain constant as the fissioning nucleus elongates. The effect on the nuclear binding energy of these deformation differences is found to be approximately 1.5 MeV, with fluctuations of the order of 1 MeV. Clearly, these numbers are not negligible compared to typical fission barrier heights.

As mentioned earlier, macroscopic-microscopic calculations of potential energy surfaces of fissioning nuclei assume equal deformations of protons and neutron distributions. In view of the above results, one is tempted to infer that these calculations predict fission barriers that are systematically  $\simeq 1$  MeV too high. One must note that only the fluctuating part of  $\delta E_{\text{den}}$  can actually influence barrier heights calculated with the macroscopic-microscopic approach, since the average value of this difference can be taken into account in the fitting of the parameters of the macroscopic (e.g. liquid drop) model. Still, as shown above, neglecting neutron-proton deformation differences can induce an overestimation of spontaneous fission lifetimes by several orders of magnitude in heavy and superheavy nuclei.

This result suggests that it might be useful to generalize the currently used macroscopic-microscopic approaches in order to allow protons and neutrons to have different multipole deformations. One could start from the energy prescription :

$$E_{\text{Strut}}(\{\beta_\lambda^p\}, \{\beta_\lambda^n\}) = E_{\text{macr}}(\{\beta_\lambda^p\}, \{\beta_\lambda^n\}) + \delta E_{\text{micr}}^p(\{\beta_\lambda^p\}) + \delta E_{\text{micr}}^n(\{\beta_\lambda^n\}) \quad (6)$$

where both the macroscopic and and microscopic components depend on proton and neutron deformations. Then, performing a minimization with respect to e.g., the neutron multipole deformations while keeping proton deformations as independent variables, should give a more realistic description of potential energy surfaces. Details of such a method as, for instance, the way to generalize macroscopic models in order to include different deformations for protons and neutrons, are left for future study.

This work is partially financed by the Polish Committee of Scientific Research under Contract No. 2 P03B 011 12.

---

[1] C.J. Batty, E. Friedman, H.J. Gils, and H. Rebel, *Adv. Nucl. Phys.* **19**, 1 (1989).  
[2] D. Gogny, Proc. Int. Conf. on "Nuclear self-consistent fields", Trieste, 1975, p. 333.  
[3] P. Quentin and H. Flocard, *Ann. Rev. Nucl. Part. Sci.* **28**, 523, (1978).  
[4] J. Dechargé and D. Gogny, *Phys. Rev.* **C21**, 1568 (1980).  
[5] A. Baran, J. L. Egido, B. Nerlo-Pomorska, K. Pomorski, P. Ring, and L. M. Robledo, *J. Phys.* **G21**, 657 (1995).  
[6] K. Pomorski, P. Ring, G. A. Lalazissis, A. Baran, Z. Łojewski, B. Nerlo-Pomorska, and M. Warda, *Nucl. Phys.* **A624**, 349 (1997).  
[7] M. Warda, B. Nerlo-Pomorska, and K. Pomorski, *Nucl. Phys.* **A635**, 484 (1998).  
[8] Z. Patyk, A. Baran, J.F. Berger, J. Dechargé, J. Dobaczewski, and A. Sobiczewski, *Phys. Rev.* **C59**, 704 (1999).  
[9] D. Gogny, in Proc. Int. Conf. on "Nuclear Physics with Electromagnetic Interactions", Mainz (Germany), 1979.  
[10] M. Girod and D. Gogny, *Phys. Lett. B* **64** (1976) 5.  
[11] M. Girod and P.G. Reinhard, *Phys. Lett. B* **117**, 1 (1982).  
[12] B. Nerlo-Pomorska and K. Pomorski, *Z. Phys.* **A344**, 359 (1993).  
[13] B. Nerlo-Pomorska and K. Pomorski, *Z. Phys.* **A348**, 169 (1994).

- [14] Z. Lojewski, B. Nerlo-Pomorska, K. Pomorski, and J. Dudek, Phys. Rev. **C51**, 601 (1995).
- [15] J.F. Berger, M. Girod, and D. Gogny, Nucl. Phys. **A502**, 85c (1989).
- [16] Z. Lojewski and A. Staszczak, Nucl. Phys. **A657**, 134 (1999).
- [17] R. Smolańczuk, J. Skalski, and A. Sobiczewski, Phys. Rev. **C52**, 1871 (1995).
- [18] P. Moeller, J.R. Nix, W.D. Myers, and W.J. Swiatecki, Atomic Data Nucl. Data Tables **59**, 185 (1995).
- [19] J.F. Berger, M. Girod, and D. Gogny, Comp. Phys. Comm. **63**, 365 (1991).
- [20] M. Girod and B. Grammaticos, Nucl. Phys. **A330**, 40 (1979).
- [21] J. Randrup, S.E. Larsson, P. Moeller, S.G. Nilsson, K. Pomorski, A. Sobiczewski, Phys. Rev. **C13** (1976) 229.

## Figure captions

1. Fission barriers of  $^{232}\text{Th}$ ,  $^{236}\text{U}$ ,  $^{238}\text{U}$  and  $^{240}\text{Pu}$  obtained with the HFB method and the Gogny effective interaction. They are drawn as functions of the nucleus total (mass) quadrupole moments. Center of mass, rotational and vibrational corrections are included, as explained in the text. The solid lines represent the fission barriers for reflection symmetric shapes, while the dashed lines correspond to asymmetric fission.
2. Multipole deformations  $\beta_\lambda$ ,  $\lambda = 2,3,4$  of the  $^{232}\text{Th}$  density (upper left), and the differences  $\beta_\lambda^n - \beta_\lambda^p$  between neutron and proton multipole deformations for symmetric (solid curves) and asymmetric (dashed curves) fission of  $^{232}\text{Th}$ , as functions of the total quadrupole moment.
3. Differences between the fission barriers obtained with and without constraint (5) imposing equal deformations to neutrons and protons, in  $^{232}\text{Th}$ ,  $^{236}\text{U}$ ,  $^{238}\text{U}$  and  $^{240}\text{Pu}$ .
4. Fission barriers for the asymmetric fission of  $^{232}\text{Th}$ ,  $^{236}\text{U}$ ,  $^{238}\text{U}$  and  $^{240}\text{Pu}$ , obtained with (dashed curves) and without (solid curves) constraint (5) imposing equal deformations to neutrons and protons. The dashed curves are shifted downward in order that ground state minima coincide.

FIG. 1.

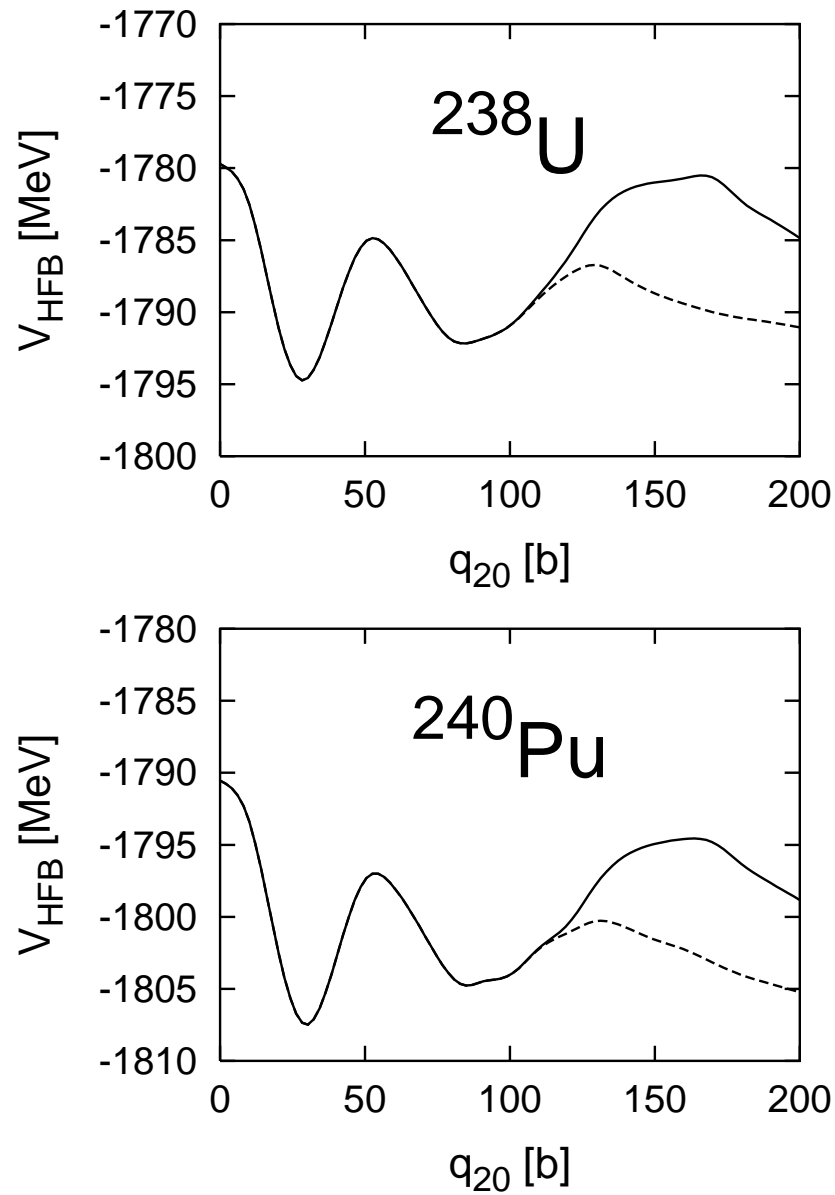
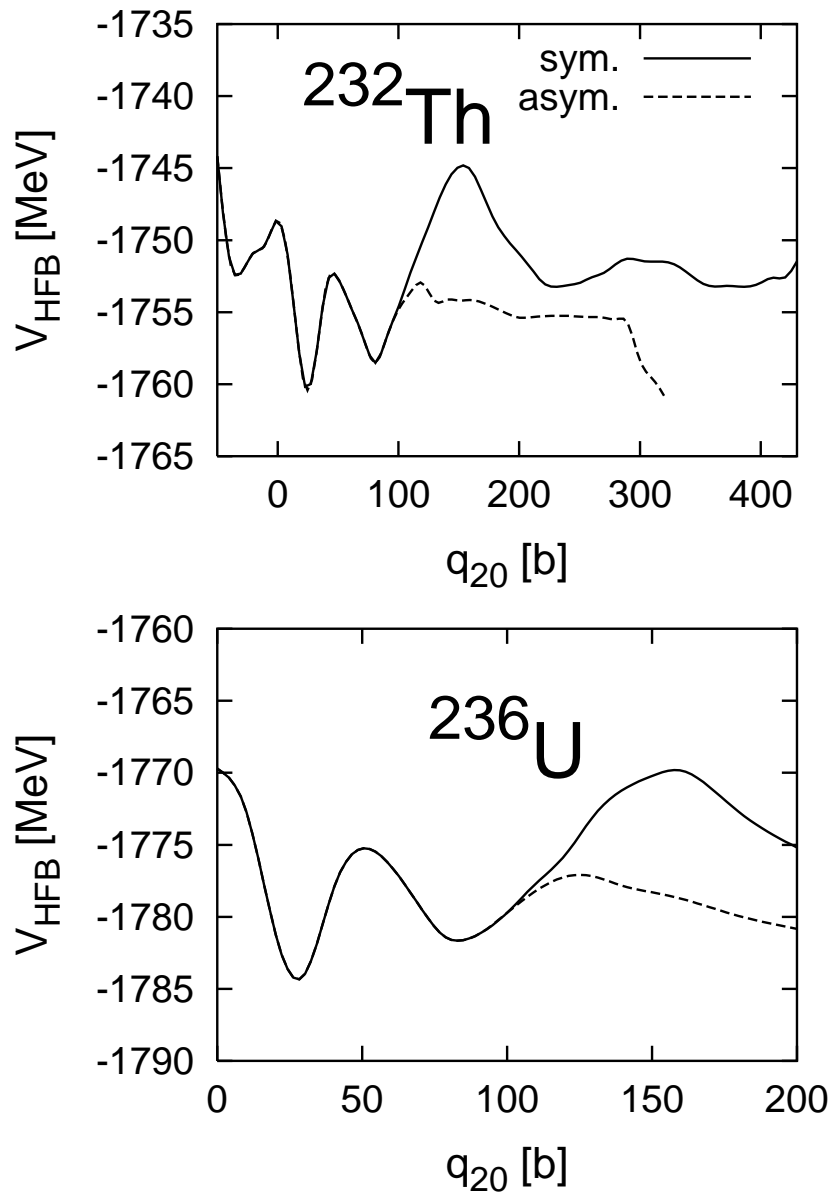


FIG. 2.

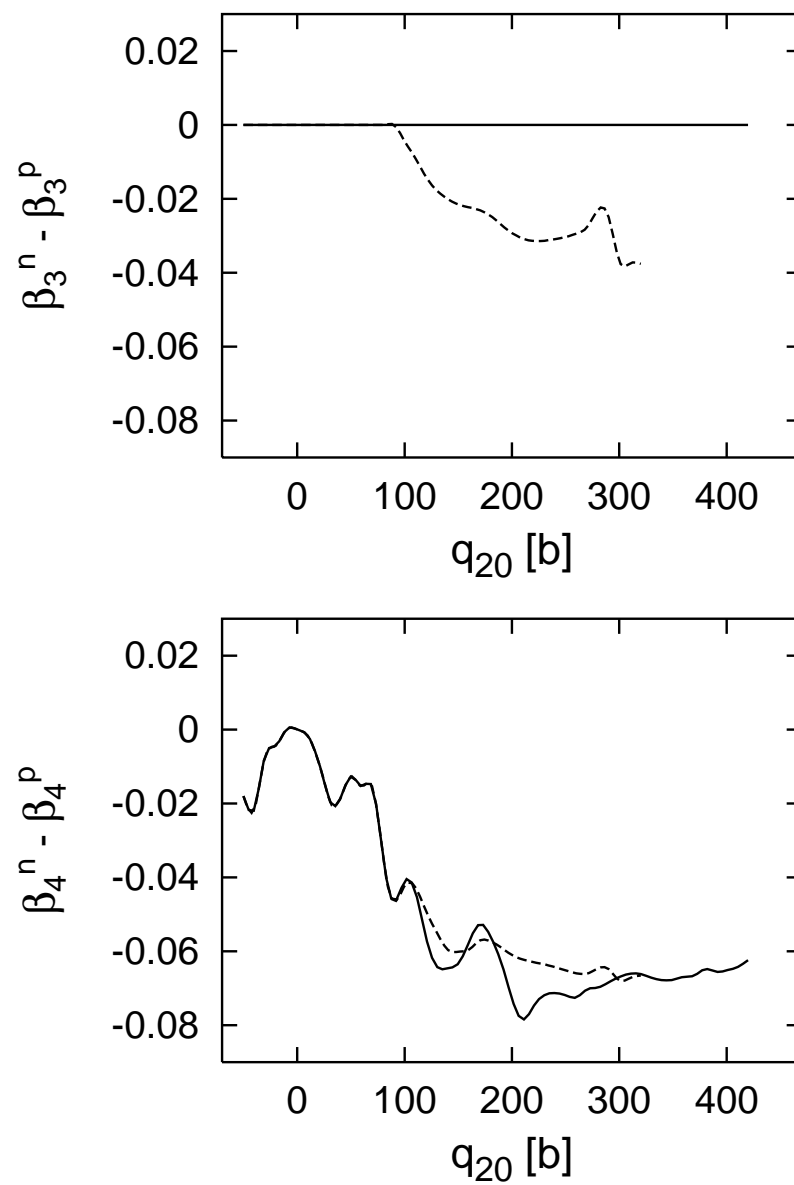
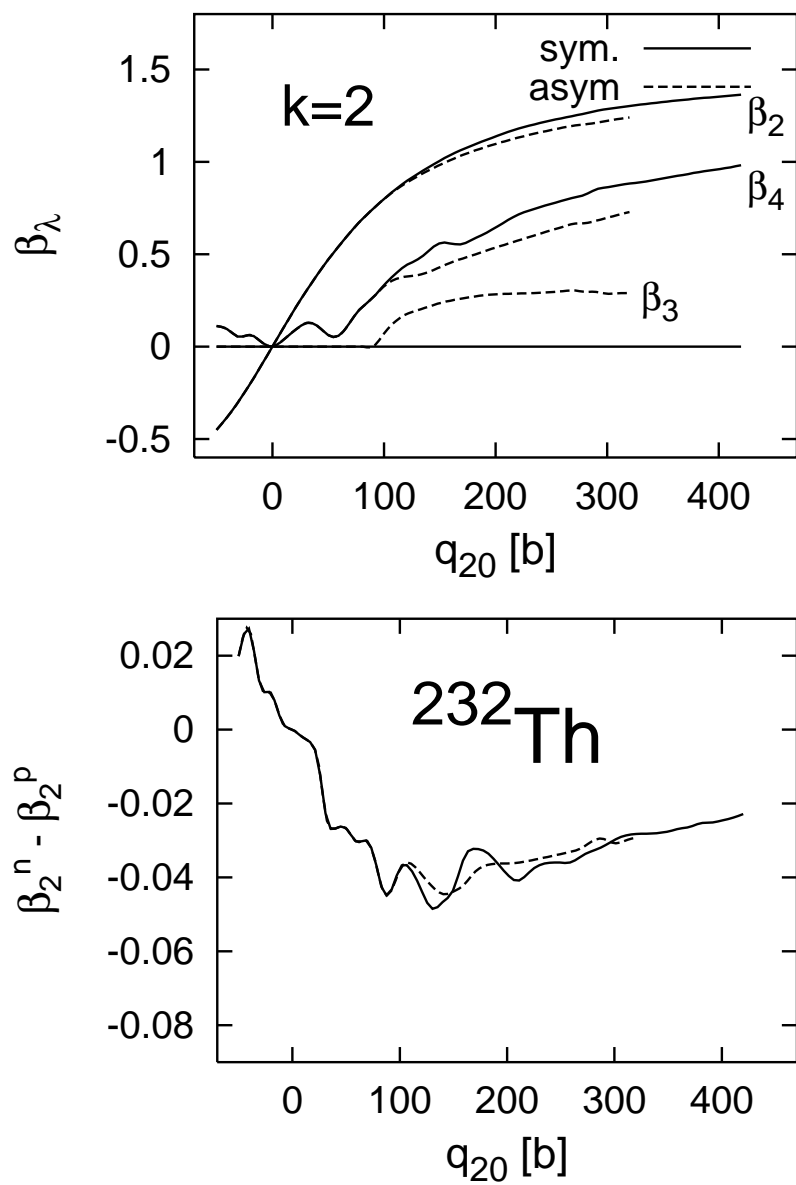


FIG. 3.

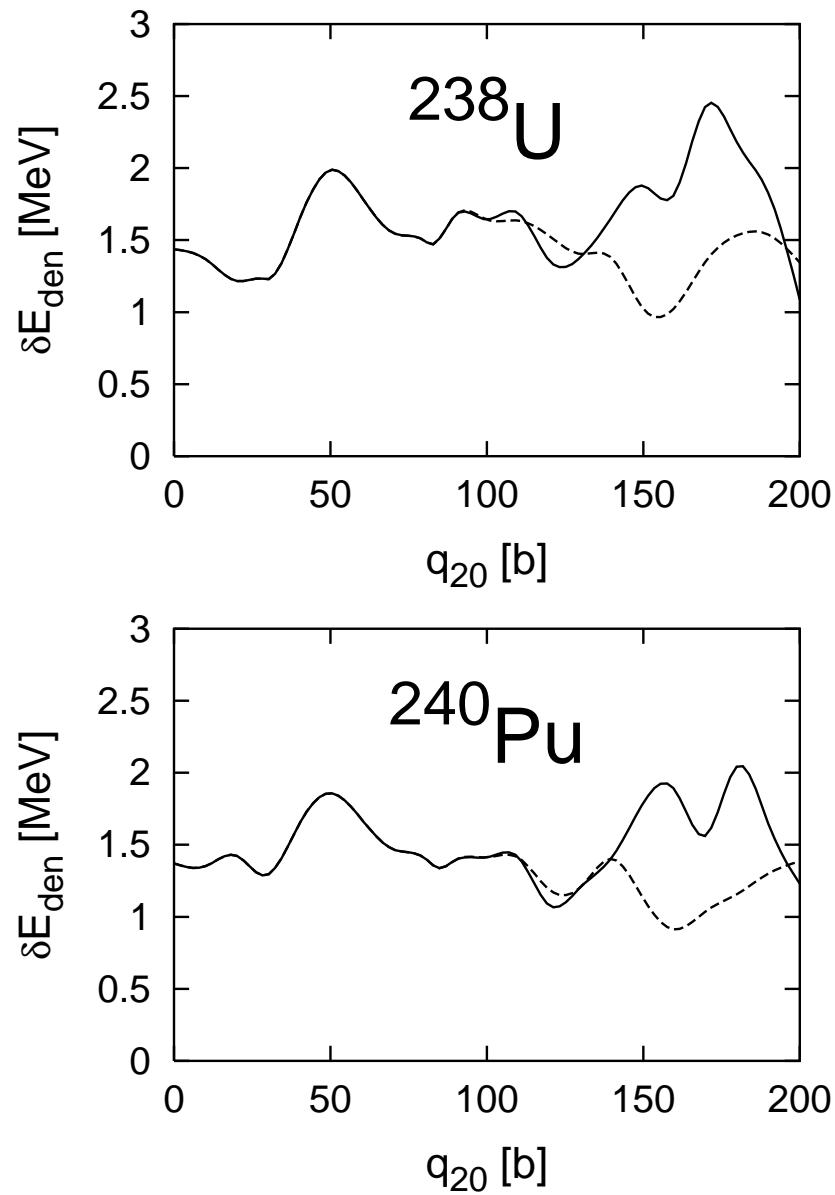
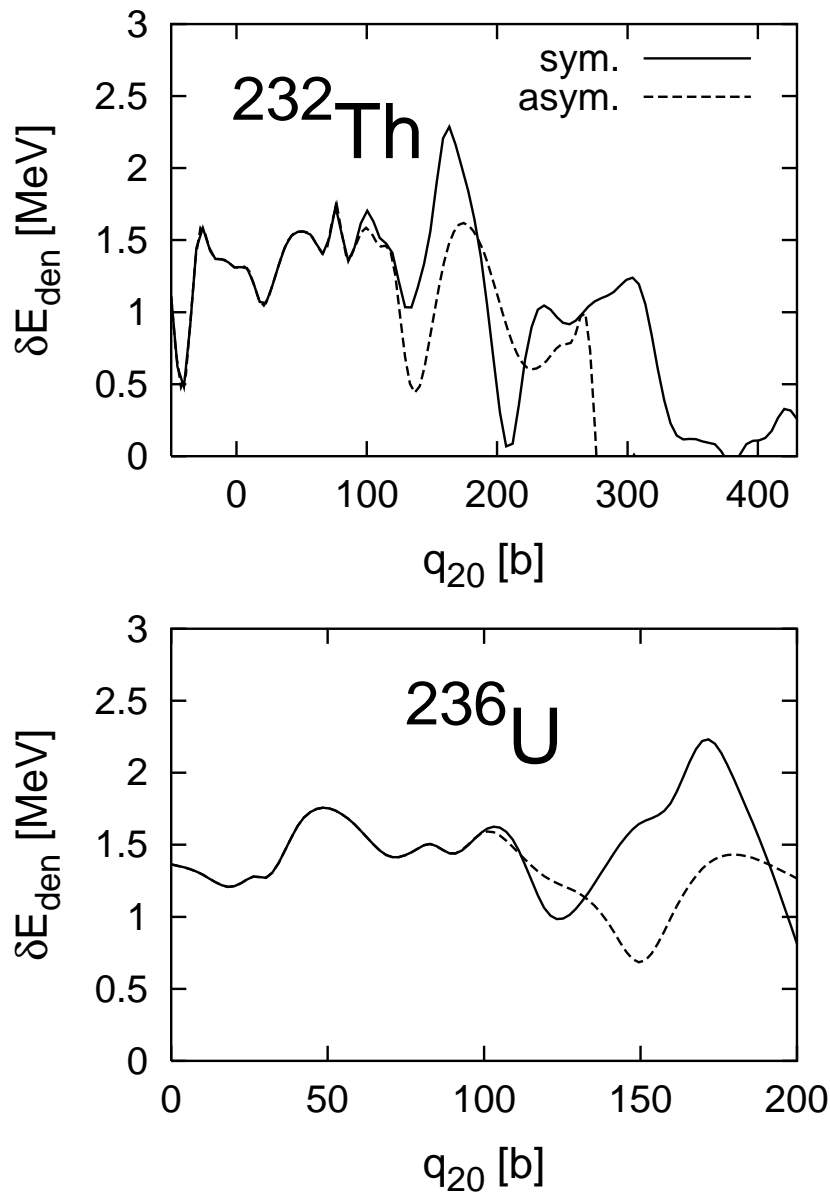


FIG. 4.

